Journal of Rock Mechanics and Geotechnical Engineering xxx (xxxx) xxx

Contents lists available at ScienceDirect

Journal of Rock Mechanics and Geotechnical Engineering

journal homepage: www.jrmge.cn

Full Length Article

Effects of freeze-thaw cycles on sandstone in sunny and shady slopes

Dian Xiao [a,b,c], Xiaoyan Zhao [b,*], Corrado Fidelibus [d], Roberto Tomás [c], Qiu Lu [b], Hongwei Liu [b,e]

[a] China Academy of Railway Sciences Corporation Limited, Beijing, China
[b] Faculty of Geosciences and Environmental Engineering, Southwest Jiaotong University, Chengdu, China
[c] Department of Civil Engineering, University of Alicante, Alicante, Spain
[d] Department of Innovation Engineering, University of Salento, Lecce, Italy
[e] Department of Earth and Environmental Sciences, University of Milano Bicocca, Milan, Italy

ARTICLE INFO

Article history:
Received 6 May 2023
Received in revised form
10 November 2023
Accepted 4 December 2023
Available online xxx

Keywords:
Sunny-shady slope
Freeze and thaw
Pore structure
Tight rocks
Talus slope
Cold regions

ABSTRACT

A growing rock engineering activity in cold regions is facing the threat of freeze-thaw (FT) weathering, especially in high mountains where the sunny-shady slope effects strongly control the difference in weathering behavior of rocks. In this paper, an investigation of the degradation of petrophysical characteristics of sandstone specimens subjected to FT cycle tests to simulate the sunny-shady slope effects is presented. To this aim, non-destructive and repeatable testing techniques including weight, ultrasonic waves, and nuclear magnetic resonance methods on standard specimens were performed. For the sunny slope specimens, accompanied by the enlargement of small pores, 100 FT cycles caused a significant decrease in P-wave velocity with an average of 23%, but a consistent rise of 0.18% in mass loss, 34% in porosity, 67% in pore geometrical mean radius, and a remarkable 14.5-fold increase in permeability. However, slight changes with some abnormal trends in physical parameters of the shady slope specimens were observed during FT cycling, which can be attributed to superficial granular disaggregation and pore throat obstruction. Thermal shocks enhance rock weathering on sunny slopes during FT cycles, while FT weathering on shady slopes is restricted to the small pores and the superficial cover. These two factors are primarily responsible for the differences in FT weathering intensity between sunny and shady slopes. The conclusions derived from the interpretation of the experimental results may provide theoretical guidance for the design of slope-failure prevention measures and the selection of transportation routes in cold mountainous regions.

1. Introduction

In the rock formations of cold mountain regions, the freeze-thaw (FT) cycling of the water in pores and fissures leads to fatigue damage caused by the induced pressure cycles (Qin et al., 2018), with associated deterioration of the microstructure and mechanical parameters (Mousavi et al., 2020a, b; Sardana et al., 2022b). As one of the primary rock weathering agents, FT cycling restricts the engineering applicability of rocks in cold regions (Sardana et al., 2022a). Slope instabilities and landslides may even occur, thus posing a serious risk for infrastructures and local collectivities (Matsuoka and Sakai, 1999; Park et al., 2015; Al-Omari et al., 2015; Li et al., 2018b, 2019).

Many researchers conducted assessments on the FT resistance of various rocks under generic climatic conditions in consideration of the physico-mechanical features (Özbek, 2014; Freire-Lista et al., 2015; Mousavi et al., 2019; Mousavi and Rezaei, 2022). However, specific micro-environmental factors, such as slope aspects, may influence the extent of FT deterioration in rocks as well. Talus slopes are common landforms in cold mountain areas that experienced periglacial climate and glaciation. On a Sunny (south-facing) Slope (SuS), the maximum ground temperatures and the seasonal temperature excursions are much higher than those on a Shady (north-facing) Slope (ShS). Consequently, the relative grain distributions of the superficial rock on the talus considerably vary from sunny slopes to shady slopes (Fig. 1). Such marked differences are the cause of a different proneness to instability (Luo et al., 2018). That is to say, the excursions of the slope aspects, represented by the temperature, and driving the FT cycles, are of paramount

* Corresponding author.
E-mail address: xyzhao2@swjtu.cn (X. Zhao).
Peer review under responsibility of Institute of Rock and Soil Mechanics, Chinese Academy of Sciences.

https://doi.org/10.1016/j.jrmge.2023.12.023

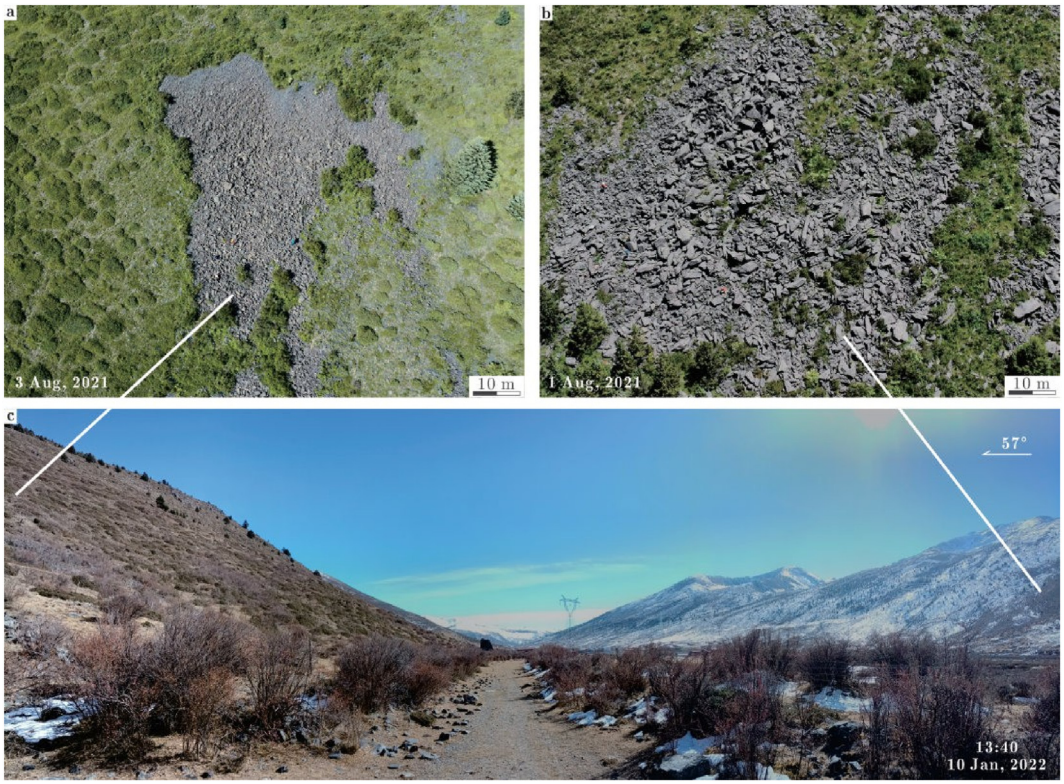

Fig. 1. Grain distribution of the superficial rock (a) of a sunny slope, and (b) of a shady slope; (c) View of a sunny slope and corresponding shady slope. The aspects of two slopes are 223° and 356°, respectively.

importance for the estimation of the associated damage (Fang et al., 2018; Abdolghanizadeh et al., 2020).

Microscopically, FT-induced damage consists of an expansion of existing pores, generation of new cracks, and propagation of fractures (Jia et al., 2020; Verma et al., 2023). Investigations concerning the evolution of such phenomena are effective in defining the resistance to FT cycles of the rock formations involved (Sun et al., 2020; Gao et al., 2023). P-wave velocity v_p (Momeni et al., 2016), scanning electron microscopy (SEM) images (Lin et al., 2020; Guler et al., 2021), and nuclear magnetic resonance (NMR) (Zhang et al., 2004; De Kock et al., 2015; Wang et al., 2020) are effective means to detect the deterioration of pore structure. By comparing the microscopic damage differences in rocks subjected to FT cycles on sunny slopes (SuS-FT cycles) and shady slopes (ShS-FT cycles), valuable indications can be obtained for a better understanding of the sunny-shady slope effects on rock FT weathering. Conclusions can also provide references for the stability evaluation of talus slopes in cold mountain regions regarding the perspective of slope aspects.

To this aim, the results of laboratory experiments on intact rock specimens of Jiaguan sandstone and the relative interpretation are reported. The specimens were split in half into two categories: the specimens subjected to SuS-FT cycles and the specimens subjected to ShS-FT cycles. The experiments include non-destructive and repeatable testing methods for the analysis of the induced damage through the measurement of mass loss, P-wave velocity, porosity, pore size distribution, and pore radius. The interpretation of the results refers to the variations of such quantities with the number N of FT cycles. The differences between the results of the two categories are emphasized and analyzed.

2. Rock features and experimental setup

The material for the experiments was collected by a core of intact Jiaguan sandstone, a brownish-red rock belonging to the Upper Cretaceous, in the Hengduan Mountain, eastern margin of the Tibetan Plateau, China. The sandstone contains fine-grained feldspar, quartz, and lithic fragments, floating within the mud-to a silt-sized matrix, classified as *wackes* (Fig. 2a). Clays in the matrix are comprised of illite, mixed-layer illite/smectite, and chlorite (Fig. 2b).

Eighteen cylindrical specimens, with a diameter of 50 mm and a height of 100 mm, were cut from the fetched core using a diamond drill rig, conforming to the Chinese code GB/T 50266-2013 (2013). Sixteen of them were divided into two groups: the sunny-slope (SuS) group and the shady-slope (ShS) group. They were then ordered with a number from 1 to 8 separately in a way that specimens with the same given number have similar porosity values. The initial physico-mechanical properties are reported in Table 1. Two remaining specimens were used for temperature monitoring during SuS-FT and ShS-FT cycles, respectively. The surface and core temperatures were recorded in each specimen by means of two measuring devices, one placed on the end face and one in a hole, drilled parallel to the axis.

The following experiments were performed on the specimens SuS1–8 and ShS1–8: SEM observations on SuS1–4 and ShS1–4, measurements of mass loss Δm, P-wave velocity v_p, porosity ϕ, and NMR parameters on SuS5–7 and ShS5–7, definition of NMR transverse surface relaxation time T_2 spectra on layered on SuS8 and ShS8.

Rocks in Hengduan Mountain undergo 25–30 FT cycles per year. Given the prolonged exposure of rocks to surface environments,

Please cite this article as: Xiao D et al., Effects of freeze-thaw cycles on sandstone in sunny and shady slopes, Journal of Rock Mechanics and Geotechnical Engineering, https://doi.org/10.1016/j.jrmge.2023.12.023

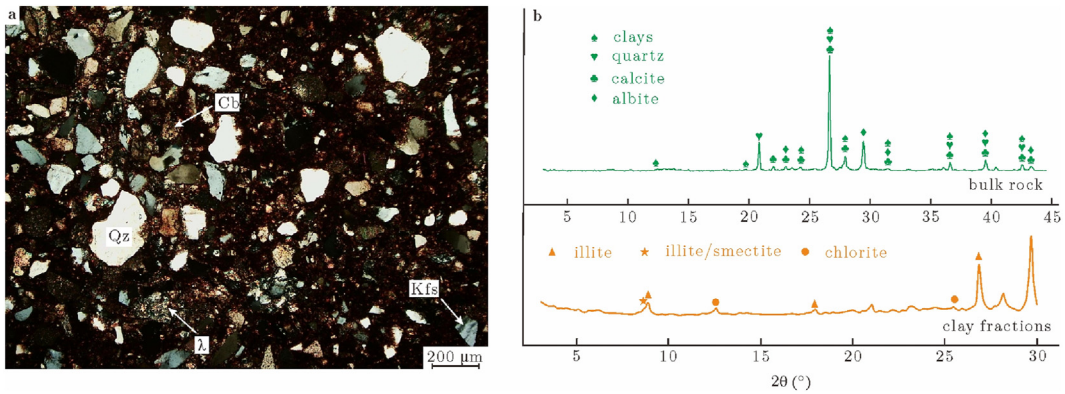

Fig. 2. (a) Thin-section micro-photograph taken under crossed Nicols (Qz - quartz, Kfs - potassium feldspar, Cb - carbonate mineral, λ - rhyolite); and (b) XRD patterns (bulk rock and air-dried clay fractions) of the Jiaguan sandstone.

this study employed 25, 50, 75 and 100 FT cycles to reproduce 1–4 years of FT weathering. The number N of FT cycles for each specimen and the synopsis of the experiments are reported in Table 2. A scheme of the procedure adopted for the experiments is shown in Fig. 3.

2.1. FT cycles

In cold regions, pore water inside the rocks is mainly supplied by the melting snow. Hillside rocks can be found, at least temporarily, in full saturation conditions, frequently at the edge of a snowfield, even in dry mountainous areas (Sass, 2005).

The specimens subjected to the experiments were all fully saturated, since the greatest damage caused by FT-cycles-induced develops under these conditions. The saturation was performed under vacuum conditions for 8 h until no bubbles spat out, then the specimens were left submerged for 24 h. Afterward, the saturated specimens were wrapped in plastic films to maintain the moisture content.

In this study, the temperature range set for the SuS-FT cycles was −20 °C to 20 °C, according to the local meteorological conditions of the sunny slope in Hengduan Mountain. This temperature fluctuation also meets the requirements of Chinese code GB/T 50266-2013 (2013). Concerning that the maximum daily temperature of sunny slope is about 15 °C higher than that of shady slope, the temperature range set for the ShS-FT cycles was −20 °C to 5 °C. In addition, given that in winter the shady slopes are usually covered by snow (Fig. 1), which functions as isolation material, a polystyrene foam was used to wrap specimens ShS1–8 to better reproduce the temperature evolution inside the rock of shady slopes.

The FT cycles were performed in automatic environmental cabins (MIT-80L). Each FT cycle took 520 min, with time periods equal for freezing and thawing. Furthermore, the cooling rate and the heating rate were both equal to 2 °C/min.

2.2. SEM observations

SEM observations were carried out on 1 × 0.5 cm^2 slabs, which were cut from the upper top of specimens SuS1–4 and ShS1–4 after the given numbers of cycles per specimen (Table 2). All the slabs were polished and then cleaned with alcohol. The surface was sputter-coated with 10 nm-thick gold film prior to the analysis to enhance the conductivity and improve the clarity of observation. Images were acquired using a JSM-IT500 scanner with 15 kV accelerating voltage, a working distance of 10–12 mm, and observations performed in secondary electron mode.

2.3. NMR tests

In an NMR test, the transverse magnetization vector intensity M is proportional to the number of protons n_p contained in the pore-filling fluids, and the transverse relaxation time T_2 is mainly influenced by the pore structure (Yang et al., 2021). A proportionality between T_2 and the pore radius r is applicable:

$$\frac{1}{T_2} \simeq \rho_2 \frac{S}{V} = \rho_2 \frac{F_s}{r} \tag{1}$$

where S is the pore surface area; V is the pore volume; ρ_2 is the transverse surface relaxivity, specific property of the rock; and F_s is the pore shape factor. For sandstones, $\rho_2 F_s$ is equal to 0.01 μm/ms (Jia et al., 2020).

The NMR measurements of SuS5–7 and ShS5–7 every 25 FT cycles were performed using a low-field AniMR-150 NMR system, with the magnetic field intensity of 0.23 T (1 T = kg/(s^2 A)) and a hydrogen proton Larmor frequency of 12.8 MHz. Layered T_2 spectra for SuS8 and ShS8 were conducted using the MacroMR12-110H-GS-HTHP NMR system. Each specimen was spatially divided into nine layers. The magnetic field intensity was 0.29 T with a hydrogen proton Larmor frequency of 12 MHz.

2.4. Measurement of physical properties

The mass loss Δm was calculated after N FT cycles (with N equal to 0, 25, 50, 75 and 100, see Table 2) through the following equation:

$$\Delta m = \frac{m_{d0} - m_{dN}}{m_{d0}} \tag{2}$$

where m_{d0} is the initial dry mass of a specimen, and m_{dN} is the dry mass after N FT cycles. The accuracy of the balance is 0.01 g.

The porosity ϕ was determined with the conventional laboratory gravimetric method by applying the following equation:

$$\phi = \frac{m_{sat} - m_d}{\rho_w V_{ts}} \tag{3}$$

where m_{sat} and m_d are the masses of the saturated specimen and the dry specimen, respectively; ρ_w is the water density; and V_{ts} is the volume of the tested cylindrical specimen. The parameter was

Please cite this article as: Xiao D et al., Effects of freeze-thaw cycles on sandstone in sunny and shady slopes, Journal of Rock Mechanics and Geotechnical Engineering, https://doi.org/10.1016/j.jrmge.2023.12.023

Table 1
Initial values of physico-mechanical properties for specimens.

Label	ρ_d (g/cm^3)	v_p (m/s)	ϕ (%)	UCS (MPa)
SuS	2.48–2.59	2844–3831	2.98–4.94	74–97
ShS	2.47–2.60	2968–3808	2.98–5.39	

Table 2
Number of FT cycles and cycles after which the observations and experiments were performed.

Label	Number of cycles	Number of observation cycles	Measured property
SuS1, ShS1	25	25	SEM observations on the slab
SuS2, ShS2	50	50	
SuS3, ShS3	75	75	
SuS4, ShS4	100	100	
SuS5, ShS5	100	0, 25, 50, 75, 100	Δm, ϕ, P-wave velocity v_p, NMR T_2 spectrum
SuS6, ShS6	100		
SuS7, ShS7	100		
SuS8, ShS8	100	0, 100	Layered NMR T_2 spectrum
SuST, ShST	100	Continuous	Temperature monitoring

also measured by resorting to the NMR tests. ϕ is proportional to the NMR signal received from a pulse sequence Carr-Purcell-Meiboom-Gill data, thus one has

$$\phi = \frac{A_{ts} V_{cal}}{A_{cal} V_{ts}} \phi_{cal} \tag{4}$$

where V_{cal} is the volume of the calibration specimen; A_{cal} and A_{ts} are the total NMR amplitudes of the calibration specimen and the tested specimen, respectively; and ϕ_{cal} is the porosity of the calibration specimen. The reliability of the porosity data was confirmed by the negligible difference between both results. The common lower value drawn from NMR measurements may be attributed to the clay-bound water in the specimens beyond the resolution of the NMR instrument (Xie et al., 2008). The ϕ values from NMR are preferentially adopted in what follows.

The P-wave velocity v_p of dry specimens was computed from the ratio between the height h of the cylindrical specimen and the mean transmission travel time t_m of an acoustic pulse along the sample axis. The geometrical mean radius r_{gm} of the pores, the permeability k, and the pore variation coefficient C, were calculated from the NMR tests. For r_{gm}, one has

$$r_{gm} = \rho_2 F_s T_{2gm} \tag{5}$$

being T_{2gm} the weighted geometrical mean of the T_2 spectrum, equal to (Qin et al., 2017):

$$T_{2gm} = \exp\left[\sum_{i=1}^{100} \frac{A_i}{A_{ts}} \ln(T_{2i})\right] \tag{6}$$

where T_{2i} is a variable relaxation time, and A_i is the amplitude corresponding to T_{2i}.

By means of the NMR spectroscopy, the permeability k of a specimen cannot be directly measured. However, an indirect estimation is available by resorting to the Schlumberger-Doll Research (SDR) model (Kenyon et al., 1988):

$$k = a T_{2gm}^2 \phi^4 \tag{7}$$

where a is a coefficient related to the rock properties, usually equal to 4 for sandstones (Rezaee et al., 2012).

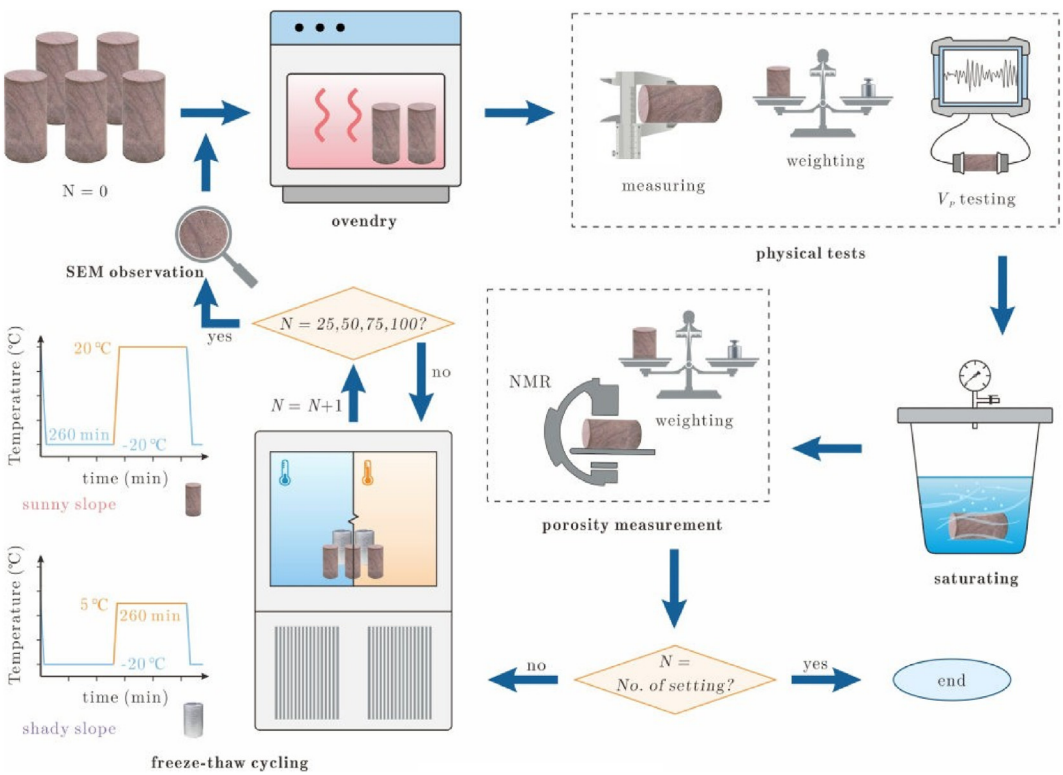

Fig. 3. Test procedure.

Please cite this article as: Xiao D et al., Effects of freeze-thaw cycles on sandstone in sunny and shady slopes, Journal of Rock Mechanics and Geotechnical Engineering, https://doi.org/10.1016/j.jrmge.2023.12.023

The change in pore structure depends to a large extent on the pore size distribution. The pore variation coefficient C is introduced herein to quantify such a change by considering the T_2 distribution. Quantity w_i is the weight of each pore size, based on the variation coefficient method. One has

$$w_i = \frac{v_i}{\sum v_i} \tag{8}$$

where v_i is the coefficient of variation for the NMR signal amplitude of each point in the T_2 spectrum during the FT-cycles. The pores of the sandstone are divided into three categories: micro-pores (less than 0.1 μm), meso-pores (between 0.1 μm and 1 μm), and macro-pores (greater than 1 μm) (Meng et al., 2021), corresponding to i from 1 to 50, 51 to 67, and 68 to 100, respectively. The weight of three categories of pores, w_{mic}, w_{mes} and w_{mac}, can thus be expressed as

$$w_{\mathrm{mic}} = \frac{v_{\mathrm{mic}}}{\sum v_{\mathrm{mic}}} \tag{9}$$

$$w_{\mathrm{mes}} = \frac{v_{\mathrm{mes}}}{\sum v_{\mathrm{mes}}} \tag{10}$$

$$w_{\mathrm{mac}} = \frac{v_{\mathrm{mac}}}{\sum v_{\mathrm{mac}}} \tag{11}$$

where v_{mic}, v_{mes} and v_{mac} are the coefficients of variation of peak area indicators for micro-pores, meso-pores and macro-pores from the T_2 spectrum during FT cycling, respectively.

Define W_i as the product of the weight of each pore size w_i and the weight of the corresponding pore categories, as follows:

$$W_i = \begin{cases} w_{\mathrm{mic}} w_i & (1 \le i < 51) \\ w_{\mathrm{mes}} w_i & (51 \le i < 68) \\ w_{\mathrm{mac}} w_i & (68 \le i \le 100) \end{cases} \tag{12}$$

The pore variation considering the pore size distribution is thereby defined with the following equation:

$$C = \frac{\sum_{i=1}^{100} A_i(N) W_i}{\sum_{i=1}^{100} A_i(0) W_i} \tag{13}$$

where C is the pore variation coefficient of the specimen, and $A_i(N)$ is the amplitude corresponding to a given T_2 relaxation time after N FT cycles.

3. Analysis of the results

3.1. Mass loss

SuS and ShS specimens exhibit the same trends in mass loss, Δm increasing slightly with the number of cycles (Fig. 4a). The increase rate (i.e. the slope of the curve) is relatively high in the initial 50 cycles, then it gradually reduces.

The differences in mass change for the sunny-shady slope effect are significant. During the FT cycles, the degradation of the SuS specimens was more pronounced, and in fact, Δm of the SuS specimens is 44%–86% larger than the one of the ShS specimens.

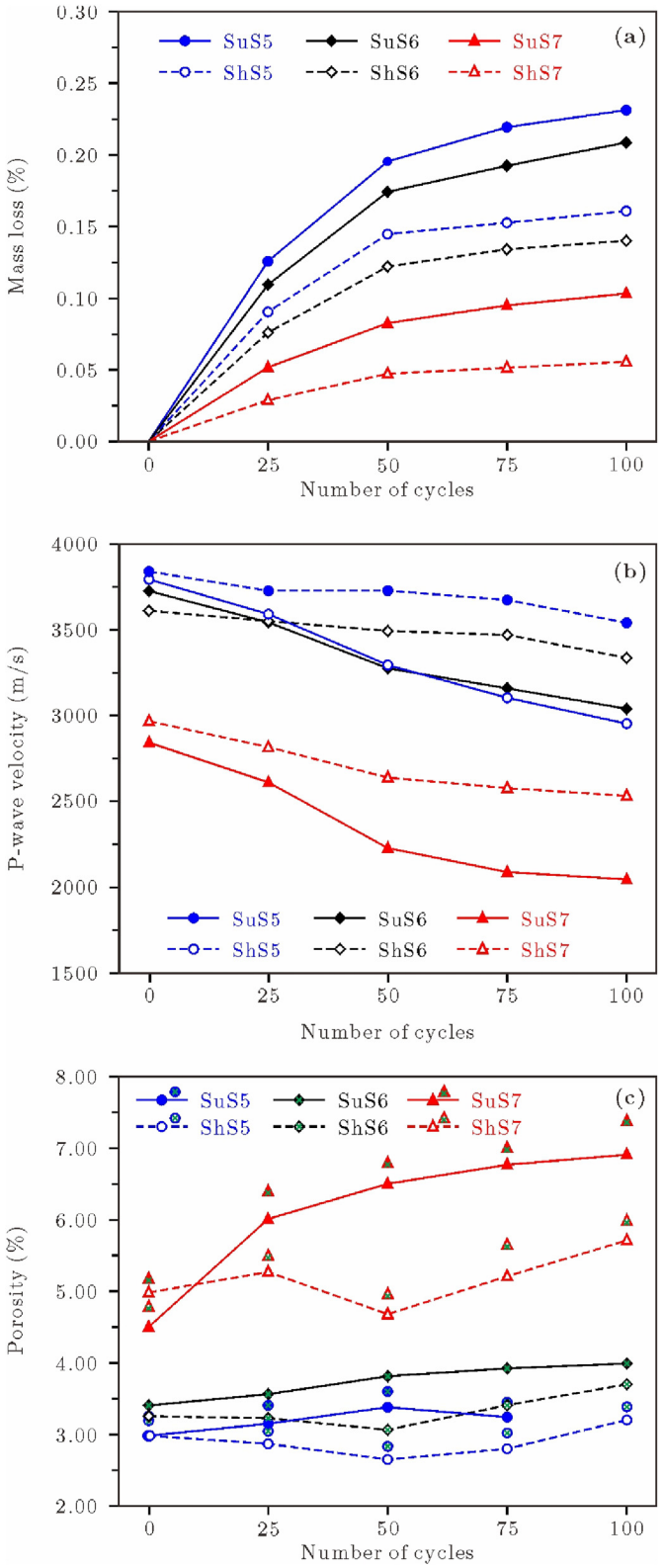

Fig. 4. Evolution of (a) mass loss Δm, (b) P-wave velocity v_p, and (c) porosity ϕ of the Jiaguan sandstone specimens subjected to FT cycles. Solid lines and dotted lines represent the evolution trends of SuS and ShS series specimens, respectively; symbols in (c) with green cross refer to ϕ values measured by means of the weighting; SuS5 was damaged by accident at the end of the test, and thereby the corresponding porosity value is unavailable.

Please cite this article as: Xiao D et al., Effects of freeze-thaw cycles on sandstone in sunny and shady slopes, Journal of Rock Mechanics and Geotechnical Engineering, https://doi.org/10.1016/j.jrmge.2023.12.023

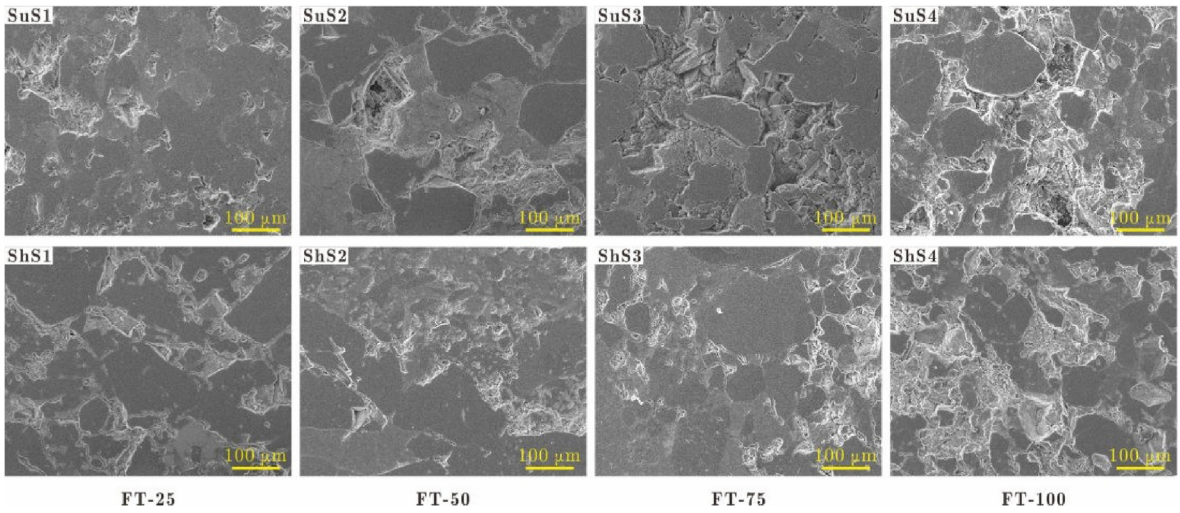

Fig. 5. SEM images showing the micro-structure evolution of the specimens of the SuS and ShS groups after FT cycling.

3.2. P-wave velocity

Ultrasonic wave velocity, as a proxy for damage, is a good indicator of the degradation due to FT weathering, regardless of the type of rock. Unlike the mass of the specimens, a notable decrease of v_p in the dry state ranging from 7.6% to 28.1% was observed after the FT cycles. Specimens SuS5 and ShS6 exhibited the maximum and minimum changes, dropping from 3800 m/s to 2954 m/s, and from 3611 m/s to 3338 m/s, respectively (Fig. 4b). The average slope of the relationship between the number of FT cycles and v_p is −8.1 for specimens SuS and −3.2 for the ShS.

SuS7, with the lowest initial P-wave velocity, shows drops of 28.1% in v_p, which is 1.9 times the drop of ShS7. As far as SuS5 and ShS5 are concerned, with the highest initial values, the differences increase up to 2.9 times. Since the difference in the decrease of v_p between the SuS and the ShS specimens can be correlated with the initial values, one may state that the sunny-shady slope effects are more significant in rocks with the higher v_p value, i.e. with a tighter structure.

3.3. Porosity

The evolution of ϕ for SuS-FT and ShS-FT cycles is quite different (Fig. 4c). ϕ constantly increases in the SuS specimens, except for SuS5 at the end of 75 cycles. In contrast, ϕ in the ShS specimens generally shows a gradual decline first and then increase up to the end of the cycling. Consequently, the final increment in ϕ of the SuS specimens is larger than that of the ShS specimens, especially for those having the highest values of initial ϕ.

3.4. Evolution of the micro-structure

The evolution of the micro-structure of the Jiaguan sandstone during FT weathering is represented by the SEM images of the specimens SuS1–4 and ShS1–4 (Fig. 5). It is apparent that the micro-structure degrades with the FT cycles. From SuS1 to SuS4 as well as from ShS1 to ShS4, an increase in the number of FT cycles leads to a higher density of micro-cracks and pores. More specifically, the deterioration of the ShS specimens is mainly related to the propagation of micro-cracks preferentially growing along the mineral crystals and breaking the surfaces of the particles, thus showing a slight mass loss. However, the deterioration is much fiercer for the SuS specimens. Granular disaggregation can be identified after 50 FT cycles, creating a bumpy surface on SuS2–4. This finding is consistent with the higher mass change experienced in the SuS specimens for the same number of cycles (Section 3.1).

4. Characteristics of the pore structure

4.1. Pore size distribution and geometrical mean radius

The spectrum of the relaxation signal T_2 of the Jiaguan sandstone with FT cycles is shown in Fig. 6. The specimens labeled with the same number have initially a similar T_2 spectrum. The T_2 values of the pores of the specimens are mainly distributed within the range 0.1–600 ms. There are three inflection points in the distribution curves of the specimens SuS5 and ShS5 centered approximately on 1 ms, 10 ms and 100 ms. However, the 100 ms inflection point lacks for the specimens SuS7 and ShS7. Furthermore, the peak areas of the inflection points for SuS5 and ShS5 in turn reduce, while they increase in SuS7 and ShS7.

As the T_2 relaxation time at the abscissa is related to the pore size, and the NMR signal amplitude on the ordinate stands for the pore volume, the rightward shift of the T_2 spectrum implies that FT weathering enlarges the pore size. Specifically, this also is exemplified by the drop in the main peak area of SuS5 and ShS5 corresponding to the shorter T_2 time, or the growth in the rightmost inflection point of SuS7 and ShS7.

The value of T_2 can be converted into the value of the pore radius r by using Eq. (1). Pore volume percentages for the three types of pores, i.e. micro-pores, meso-pores and macro-pores, are shown in Fig. 7. It is evident that the majority of pore volume in the Jiaguan sandstone at the original state consists of micro-pores, then subordinately by meso-pores, and macro-pores. The volumetric fraction of micro-pores in SuS specimen continuously reduces while the volumetric fraction of meso-pores and macro-pores increases with the cycles. These variations are more pronounced at the beginning. For the ShS specimens, it is worth noting that, albeit tendentially reduces in the whole tests, the volumetric fraction of micro-pores increases at the end of 50 cycles, a response in contrast with the one of the SuS specimens.

By observing the evolution of r_{gm}, it is further evident that the enlargement of the pores with the cycles, and increments of r_{gm} of the SuS specimens are fiercer than those of the ShS specimens (Fig. 8). For the ShS specimens, a sudden reduction in r_{gm} followed

Please cite this article as: Xiao D et al., Effects of freeze-thaw cycles on sandstone in sunny and shady slopes, Journal of Rock Mechanics and Geotechnical Engineering, https://doi.org/10.1016/j.jrmge.2023.12.023

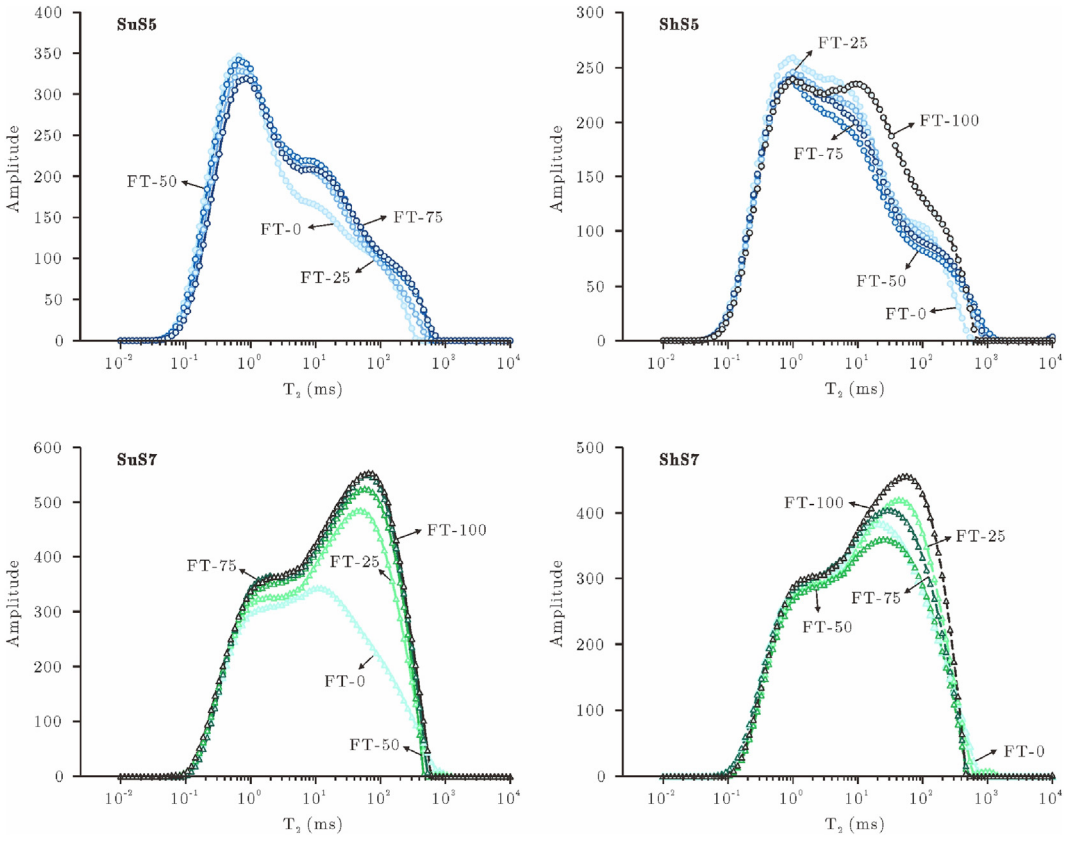

Fig. 6. T_2 spectrum distributions of the Jiaguan sandstone after different FT cycles as derived from NMR.

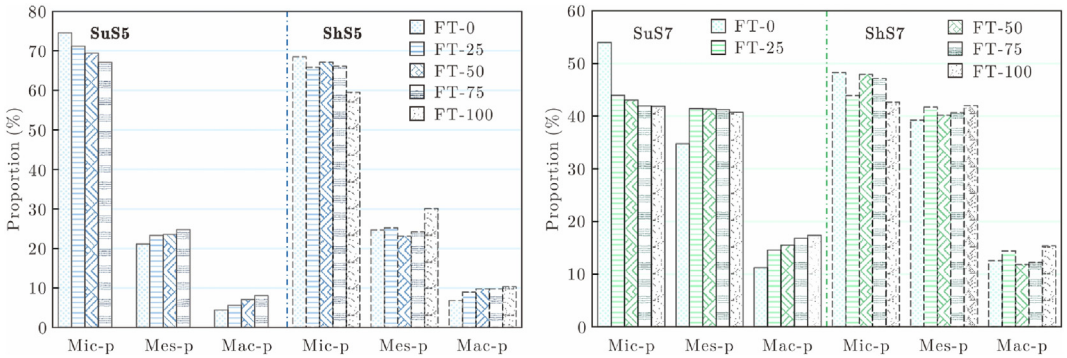

Fig. 7. NMR porosity values with the number N of FT cycles. The values for the SuS and ShS specimens are marked with solid and dashed lines, respectively (Mic-p: Micro-pores; Mes-p: Meso-pores; Mac-p: Macro-pores).

by a slow recovery is identified after 50 FT cycles, unlike the SuS specimens for which a sustained increase is observed.

4.2. Correlation C-ϕ

Micro-pores, meso-pores, and macro-pores have different weights in rock deterioration (Meng et al., 2021). In consideration of the steep increase of the weights W_i of each pore size at larger T_2 values, calculated by Eq. (8), the importance of macro-pores in pore evolution during FT weathering is confirmed (Fig. 9a).

According to Eq. (13), the pore variation coefficient C, based on the pore size distribution, evolves with FT cycle, as depicted in Fig. 9b. While a monotonic increase is observed for the SuS specimens, for the ShS specimens, a clear trend is not evident. Larger C values of the SuS specimens illustrate that they suffered a deeper FT weathering. Since large pores carry a higher weight in the calculation of C, the difference in C values between SuS and ShS specimens is predominantly attributed to the varying enlargement of the existing pores, rather than the neoformation of micro-pores.

Although ϕ exhibits an overall upward trend with FT cycles, the fluctuation does not sufficiently reflect the pore structure evolution of the studied tight sandstone during FT weathering. Precisely because C evaluates the contribution of the different pore sizes, C has an apparent correlation with FT cycles, apart from ShS7 at the end of 50 cycles. It is, therefore, considered more appropriate as an indicator of pore deterioration.

However, the evolution of C for ShS7, in line with the evolution of ϕ for the same specimen, is not characterized by a constant

Please cite this article as: Xiao D et al., Effects of freeze-thaw cycles on sandstone in sunny and shady slopes, Journal of Rock Mechanics and Geotechnical Engineering, https://doi.org/10.1016/j.jrmge.2023.12.023

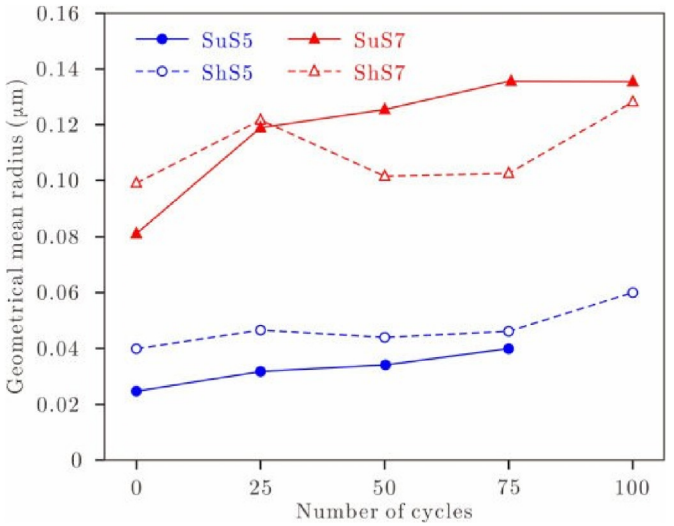

Fig. 8. Geometrical mean radius r_{gm} of the Jiaguan sandstone specimens after FT cycling.

increase, thus reflecting the superposition of multiple mechanisms leading to porosity losses. A discussion about these mechanisms is provided in Section 5.2.

5. Discussion

From the experiments, three specific issues emerged requiring a discussion: the difference in degradation among SuS and ShS specimens, the decrease of porosity, and the sunny-shady slope effect.

5.1. Difference in degradation among SuS and ShS specimens

In the experiments, to simulate the difference in FT weathering among sunny and shady slopes, the temperature ranges and the temperature change rates were differentiated. As previously mentioned, during the FT cycles, the evolution of the core and surface temperatures for the first two cycles was recorded, with reference to specimens SuST and ShST (Fig. 10).

As can be seen in Fig. 10, both time series exhibit alternating fast and slow temperature change rates. Temperature first changes on the surface, succeeded by the core of SuST and ShST in sequence. For SuST, both the surface and the core temperatures fluctuate between −20 °C and 20 °C, consistent with the ambient temperature. Conversely, for ShST, the temperature ranges are narrower than the environmental temperature range. Among them, the upper limit of the temperature of the core for ShS is only 0 °C after stabilization, indicating the incomplete melting for the pore ice near the core, and thus the FT cycles for ShS cannot be considered fully applied.

The freezing point of pore water is largely dependent on salt concentration, total stress, and pore size (Wan and Yang, 2020). Water in small pores has a lower freezing point. As the ambient temperature falls below 0 °C, water in the macro-pores freezes first, followed by the water in meso-pores and micro-pores, in that order (Ruedrich et al., 2011; Weng et al., 2021; Huang et al., 2022). The frozen pores will expand for the ice crystallization pressure (Deprez et al., 2020), leading to a reduction in the micro-pore content and an increase in the large pore content (Hou et al., 2022). In the meantime, migration of the unfrozen water outwards into other pores provides favorable conditions for the generation of new pores (Chen et al., 2004), and this always occurred, even without additional water (Huang et al., 2020), i.e. during every 25 FT cycles. However, during the thawing process, the water contained within the large pores located close to the ShST core remained frozen for a long time. Only the small pores suffer from repeated freezing and thawing in this situation. Limited water could migrate from the small pores into the tip of other micro-cracks, causing the micro-pore generation rate in ShST to be significantly lower than that in SuST.

The above inferences can be further proven by the analysis of the layered T_2 spectra of SuS8 and ShS8 before and after the whole 100 FT cycles (Fig. 11). In fact, T_2 corresponding to micro-pores in SuS8 after the FT cycles ranges from 0.142 ms to 10 ms, equal to the initial values before the tests. However, the smallest pores in ShS8 (T_2 from 0.123 ms to 3.51 ms) disappear after 100 FT cycles, which demonstrates that the micro-pores enlarged to larger pores are hardly supplemented. That is to say, the generation of newly formed micro-pores is restricted, during the FT weathering of the Jiaguan sandstone on the shady slope.

The difference between SuS and ShS specimens in the evolution of the pores was highlighted in the spatially resolved T_2 distributions. To this aim, T_2 spectra from the nine spatial locations of the two specimens shown in Fig. 11 are grouped into three parts: layers 1 to 3 as the bottom, 4 to 6 as the middle, and 7 to 9 as the top. For SuS8, the NMR signal amplitude from the top to bottom parts changes by −2%, 5.7% and 106%, respectively, after the FT cycles. Since the amplitude is proportional to the porosity of the saturated rocks, more than 90% of the increase in porosity is concentrated at the bottom of the specimen, which is indicative of the joint downward movement of water under gravity and the frost heaving

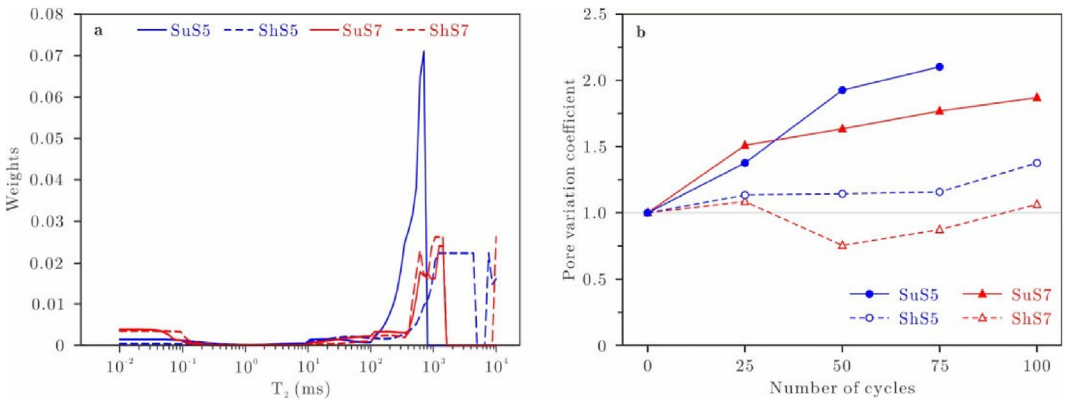

Fig. 9. (a) Weights W_i of pore size plotted against the relaxation time T_2 for the Jiaguan sandstone; and (b) Pore variation coefficient C against the number N of FT cycles.

Please cite this article as: Xiao D et al., Effects of freeze-thaw cycles on sandstone in sunny and shady slopes, Journal of Rock Mechanics and Geotechnical Engineering, https://doi.org/10.1016/j.jrmge.2023.12.023

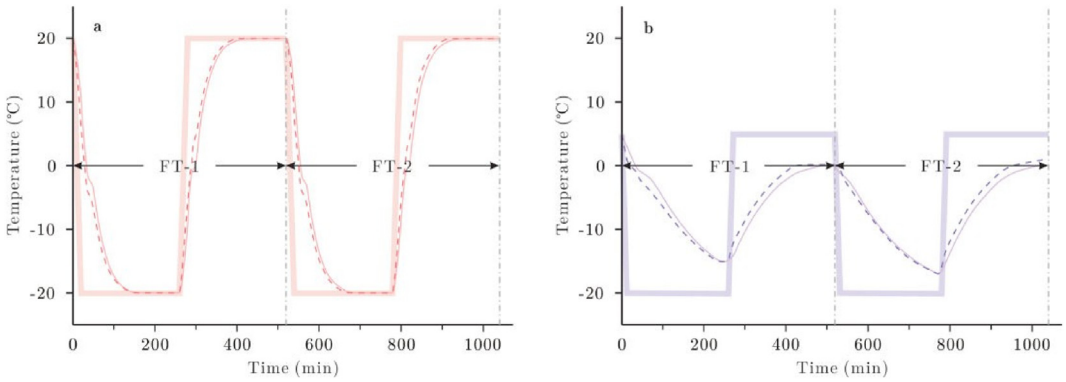

Fig. 10. Monitoring of core temperature (continuous thin line) and surface temperature (dashed thin line) for (a) SuST and (b) ShST over the first two FT cycles. The thick line represents the set temperature.

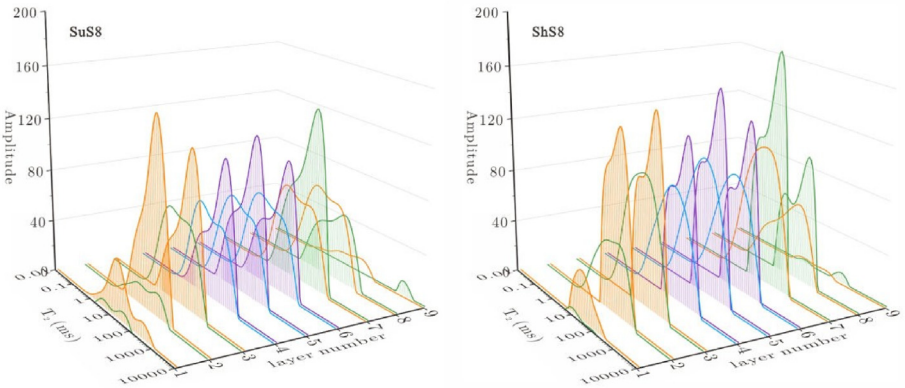

Fig. 11. Layered T_2 spectra of the Jiaguan sandstone before (solid lines) and after (solid lines with vertical stripes) 100 FT cycles. Layers 1 and 9 are at the bottom and top of the specimens, respectively.

during the long-term FT cycles. As for ShS8, for the changes in NMR amplitude, one may state that the porosity mainly grows in the lower part of the specimen, further evidence of the water penetration towards the bottom. However, the large pores near the specimen center are obstructed by ice. Therefore, the porosity of the bottom part only increases by around 30% in ShS8, in comparison with the 106% increment of the same part in SuS8, due to the restriction of pore water migration.

From the results above, it is worth noticing that the degradation of the SuS specimens was pronounced, while for the ShS specimens, the effects were mainly concentrated on the surfaces and the small pores near the cores. Therefore, as expected, the physical deterioration represented by the mass loss, the P-wave velocity, the pore structure, and the micro-structural deterioration of the SuS specimens is much more intense than that of the ShS specimens.

5.2. Porosity decrease

It is generally believed that FT cycling can alter the intrinsic pore structure in saturated rocks, enlarging the pores with an increase in porosity (Deprez et al., 2020). In the case of the Jiaguan sandstone specimens, the experienced increase is consistent in general with this evolutionary model. However, except for SuS6 and SuS7, the porosity of the remaining specimens decreased after 50 or 75 FT cycles, followed by an increase. This phenomenon was documented in other studies and attributed to particle spalling (Li et al., 2018a), pore squeeze (Liu et al., 2020), and pore obstruction (Pan et al., 2020).

FT cycles cause superficial granular disaggregation, leaving scattered sub-millimeter-scale pits on the sandstone surface (Fig. 12b). Consequently, the space previously occupied by these grains leaves new pores exposed to the air, making the total volume of pores smaller. When the exposure rate of the pores exceeds the generation and expansion rate of pores under FT cycles, the global porosity inevitably reduces. As the mass loss stabilizes after 50 FT cycles, which means that the granular disaggregation is about to cease, the porosity of the corresponding ShS specimen gradually recovers. Nevertheless, because ShS7, which presents the lowest mass loss, has the greatest porosity reduction, granular disaggregation is not the only phenomenon responsible for the porosity reduction.

Permeability k reflects the distribution and connectivity of pores inside rocks. As shown in Fig. 13, all the specimens have a small initial k value, between 10^{-5} and 10^{-2} mD. For the SuS specimens, k increases at a gradually reduced rate with the number N of FT cycles. However, for the ShS specimens, k fluctuations with N are shown. Up to 57% permeability loss of ShS7 from 25 to 50 FT cycles confirms the existence of pore obstruction.

In general, pore throats are narrow connections among pores. The effect of the FT cycles increases the connectivity. Broken particles and suspended clay in pores are free to migrate outward with the pore water through pore throats under the frost-heaving force, which is conducive to the increase of inside pore volume. This circumstance is evidentiated by the clay clumps scattering on the surface of the specimens (Fig. 12c). Nevertheless, in the ShS specimens, as mentioned in Section 5.1, the macro-pore water almost

Please cite this article as: Xiao D et al., Effects of freeze-thaw cycles on sandstone in sunny and shady slopes, Journal of Rock Mechanics and Geotechnical Engineering, https://doi.org/10.1016/j.jrmge.2023.12.023

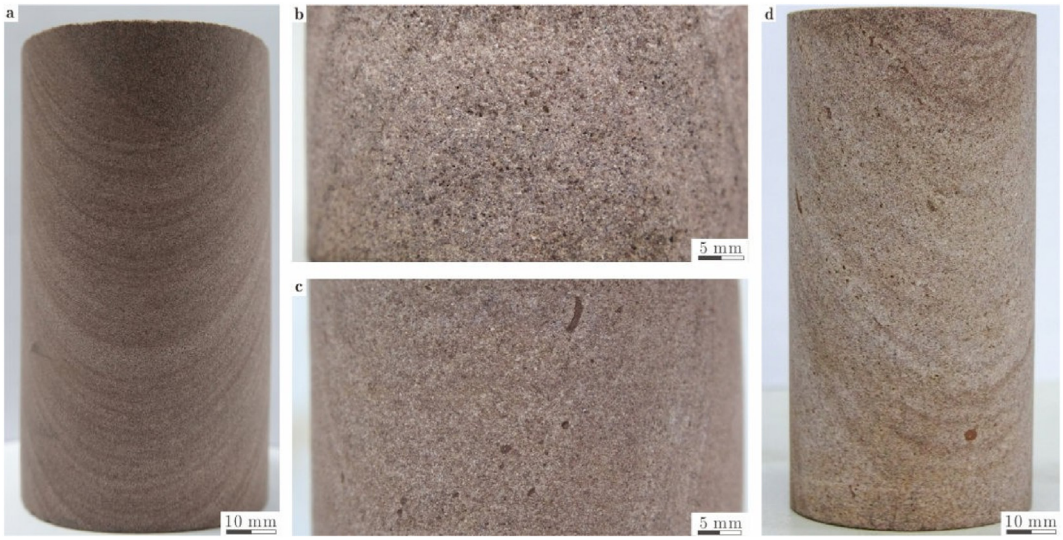

Fig. 12. Photographs of specimens (a) before and (b–d) after FT cycling.

remains frozen during the FT cycles; in other words, those pores are always filled with ice, and hence fragments are easily stuck in pore throats and block the throats, changing the open pores into closed pores. Consequently, once water cannot penetrate these pores, the porosity ϕ measured with the NMR signal or water weight is inevitably reduced, just like for the specimen ShS7 after 50 FT cycles.

Therefore, the porosity loss of the Jiaguan sandstone subjected to FT cycles can be ascribed to the superficial granular disaggregation and the pore throat obstruction.

5.3. Comparative analysis

This section conducts a comparative analysis to verify the obtained results. Extensive previous studies demonstrate that FT cycles usually cause a decrease in mass and P-wave velocity, an increase in porosity as well as the content of large pores (Park et al., 2015; Eslami et al., 2018; Sardana et al., 2022b). However, the extent of these indicator variations differs depending on the tightness of the rocks (Walbert et al., 2015; Guler et al., 2021). For porous rocks, noticeable degradation of physico-mechanical properties can be observed within short-term FT cycling (Khanlari and Abdilor, 2015; Jia et al., 2020). The sandstone in this study with low porosity and high UCS exhibited strong resistance to FT weathering. Thus, the FT cycling-induced deterioration of SuS sandstone was relatively minor. Taking the porosity as an example, a 0.59% increase in SuS6 after 100 FT cycles is similar to 0.69% in sandstone reported by Meng et al. (2021) and 0.54% in limestone by Sun et al. (2020).

In addition to the rock properties, temperature determines the appearance of frost-induced damage as well. Fang et al. (2018) concluded that the lower freezing temperature would result in more severe FT damage in sandstone. However, a paucity of research has focused on the melting temperature. Regarding the ShS specimens, since the lower melting rate and temperatures hamper the melting of pore ice, the deterioration was comparatively minimal compared with the SuS specimens. Only an average increment of 0.47% in porosity has been found after 100 FT cycles. Such a tiny increase and even decrease in porosity was also observed in Pan et al. (2020) and Momeni et al. (2016).

Overall, this study revealed the differential FT weathering characteristics of the sandstone on sunny and shady slopes from a microscale perspective. Rocks situated on sunny slopes of cold regions experience higher daytime temperatures, facing more intense FT weathering and exhibiting greater degradation. This understanding aligns with macroscopic field observations, which corresponds with descriptions in the literature by Luo et al. (2019) and Zhan et al. (2018).

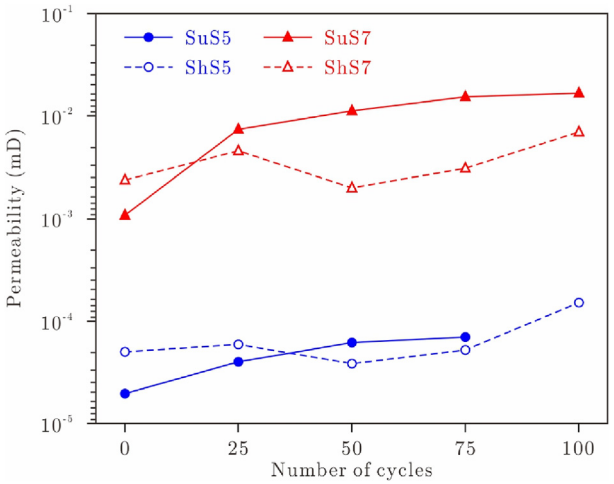

Fig. 13. NMR permeability of the Jiaguan sandstone specimens after FT cycling derived from NMR data using SDR model (Kenyon et al., 1988).

5.4. Sunny-shady slope effect

Talus slopes, as a product of weathering in alpine regions, have different characteristics according to their slope aspect (Fig. 1). These differences can be even greater for south and north orientations, where solar radiation differs by a factor of six (Auslander et al., 2003). In fact, ground temperature and change rate on sunny slopes are much higher than those on shady slopes during sunny days. When the temperature changes, differential thermal expansion and contraction inside the mineral and between adjacent mineral grains produce important inner thermal stresses (Mordovskoi and Petrov, 1994; Hale and Shakoor, 2003). Thermal

Please cite this article as: Xiao D et al., Effects of freeze-thaw cycles on sandstone in sunny and shady slopes, Journal of Rock Mechanics and Geotechnical Engineering, https://doi.org/10.1016/j.jrmge.2023.12.023

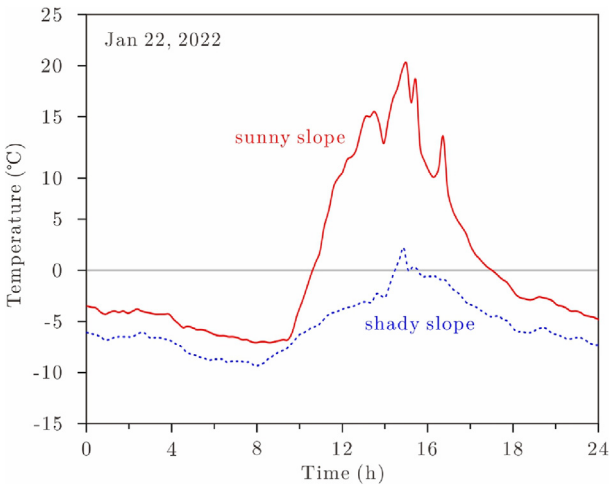

Fig. 14. Representative daily temperature variations of the surface of the sunny and shady slopes in Hengduan Mountain in winter.

stress fatigue plays also a relevant role in the weathering process of rocks at high altitude locations (Hall, 1999).

It should be noted that the larger the range and rate of temperature change, the greater the thermal stress, and thus the rock on sunny slopes accumulates more internal thermal stress and is more susceptible to fracturing in comparison to the rock on shady slopes during FT weathering.

It is worth noting that the daily maximum temperature on the surface of shady slopes in high mountain regions is only about 0 °C during winter, and lasts for very short periods due to the lack of solar radiation (Fig. 14). Therefore, as previously reported, the rocky surface of shady slopes in winter is permanently coated with snow, which acts as a thermal insulation material preventing the rock from the adverse effects of FT weathering (Fig. 1c). Even if the rock of a shady slope is subjected to FT weathering, the effects involve only the surface, preferentially the small pores.

From the analysis above, it can be stated that in sunny slopes, the FT weathering in the hillside rock is enhanced by the additional thermal stress, while in shady slopes, the intensity and depth of the FT weathering are limited (Fig. 15). For these two effects, i.e. sunny-shady slope effects, relevant differences in rock degradation substantiate.

The sunny-shady slope effect depends also on the tightness of the rock. The decline in petrophysical properties for all the specimens was rather contained, except for the P-wave velocity v_p of SuS5 and SuS6, the tightest SuS specimens (Fig. 4b). As v_p is representative of the crack density associated with the rock breakdown, the decrease in v_p of these specimens is a proof that the sunny-shady slope effect in the long term is more remarkable for tight rocks than for more porous rocks. Since for the last ones, the response to FT weathering is characterized by granular disaggregation, and being the generated fine material easily transported away from the slope, it is hard for porous rocks to form talus slopes.

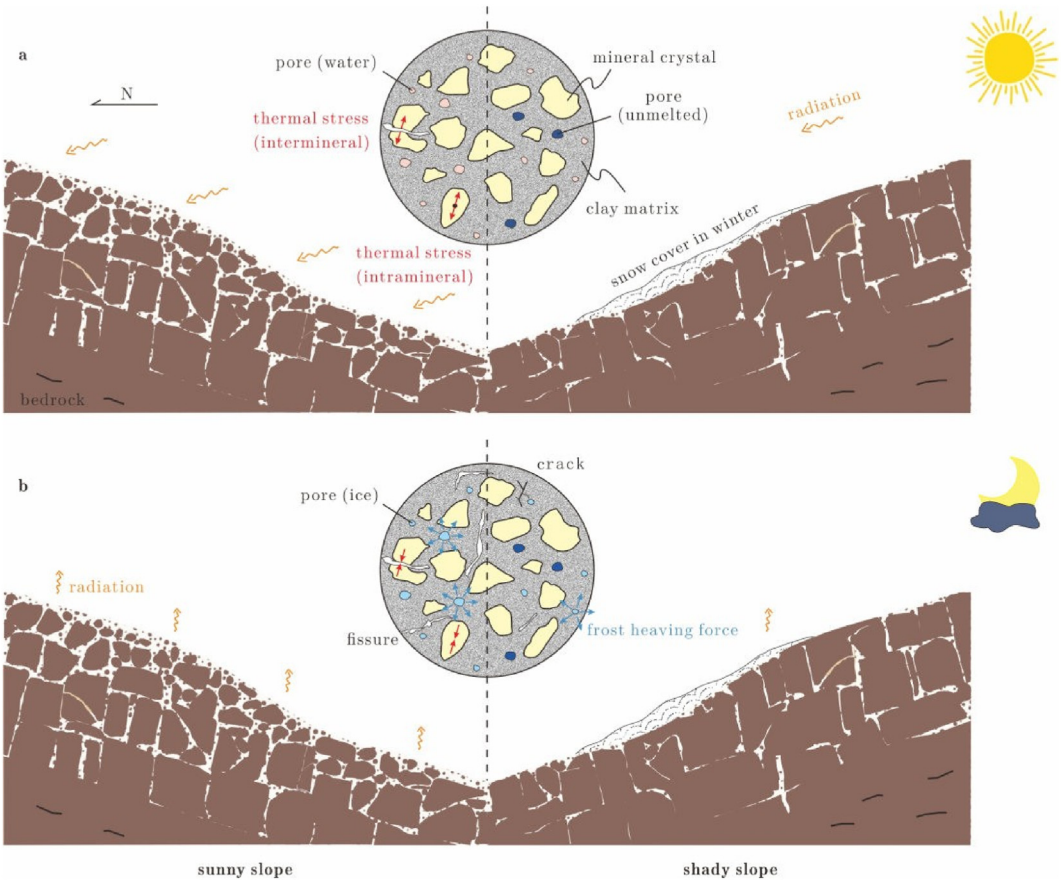

Fig. 15. Schematic overview of micro- and macro-structural evolution of FT weathering sunny-shady slope effects.

Please cite this article as: Xiao D et al., Effects of freeze-thaw cycles on sandstone in sunny and shady slopes, Journal of Rock Mechanics and Geotechnical Engineering, https://doi.org/10.1016/j.jrmge.2023.12.023

6. Conclusions

In this paper, FT cycle tests were performed on Jiaguan sandstone specimens. A series of non-destructive and repeatable testing techniques, weighting, ultrasonic, and NMR was adopted to investigate the sunny-shady slope effect under FT weathering.

In general, with the number of FT cycles, mass loss, porosity, pore geometrical mean radius, and permeability of the Jiaguan sandstone specimens increased, while the P-wave velocity decreased. There are significant differences in the degree of change of the petrophysical properties among specimens repetitively treated with simulated SuS and ShS FT cycles. Average variations in mass (0.18%), ultrasonic wave velocity (23%), porosity (34%), and pore structure of the SuS specimens are more intense, as expected, compared with those of the ShS specimens (0.12%, 10% and 12%, respectively).

The degradation of rock properties during FT cycles is accompanied by the enlargement of micro-pores into meso-pores and macro-pores. Pore variation coefficient, pore geometrical mean radius, and NMR permeability are more suitable for describing the evolution of the pore structure of the studied sandstone than the porosity. For SuS specimens, these parameters showed a decelerating growth trend with the number of FT cycles. In contrast, the response of the ShS specimens abruptly deviates from the increasing trend after 50 FT cycles.

FT weathering of ShS specimens is mainly confined to the small pores and to the areas placed near the surface. Additionally, it was also observed that the broken fragments are easily stuck in pore throats and block the throats since the water of the large pores is completely frozen during the FT weathering. This is the reason for the observed decrease in the porosity of the ShS specimens after 50 cycles, and also of the slow changes in the pore structure. By contrast, for the SuS specimens, the larger temperature difference and temperature change rate led to enhanced thermal stress (thermal shock). Therefore, the rocks of sunny slopes are subjected to an additional degradation during FT weathering, leading to a larger susceptibility to breakdown and form talus slopes than shady slopes. Consequently, sunny slopes face a higher risk of instability from a long-term perspective. By contrast, shady slopes, in which rock weathering is hampered, may be preferentially selected for example as suitable routes for railways and roads.

Although this study provides important conclusions about the FT weathering processes of rock masses, further studies and investigations will be necessary to corroborate the obtained conclusions considering other areas of study and rock types.

Declaration of competing interest

The authors declare that they have no known competing financial interests or personal relationships that could have appeared to influence the work reported in this paper.

Acknowledgments

This research was jointly supported by the National Natural Science Foundation of China (Grant No. 41672295) and the Major Systematic Project of Scientific and Technological Research and Development Plan of China Railway Corporation (Grant No. P2018G047). Dian Xiao and Hongwei Liu were supported by a PhD fellowship from the China Scholarship Council. Roberto Tomás was partially funded by the Conselleria de Innovación, Universidades, Ciencia y Sociedad Digital de la Generalitat Valenciana (CIAICO/2021/335). Thank Li Liu, Jing Tong, and Bozhou Hu for the laboratory assistance and NMR analysis. The authors also thank the editor and anonymous reviewers for their constructive comments, which greatly improved the quality of this manuscript.

List of symbols

a	Model coefficient
A_{cal}	Total NMR amplitude of the calibration specimen
A_i	NMR amplitude corresponding to t_{2i}
$A_i(N)$	A_i at the end of N FT cycles
A_{ts}	Total NMR amplitude of the tested specimen
C	Pore variation coefficient
F_s	Pore shape factor
h	Height of the specimen (m)
k	Permeability (mD)
M	Magnetization vector intensity
m_d	Mass of dry specimen (g)
m_{d0}	Initial dry mass (g)
m_{dN}	Dry mass after N FT cycles (g)
m_{sat}	Mass of saturated specimen (g)
N	Number of FT cycles
n_p	Number of protons
r	Pore radius (μm)
r_{gm}	Pore geometrical mean radius (μm)
S	Pore surface area (μm^2)
T_2	Transverse surface relaxation time (ms)
T_{2gm}	Weighted geometrical mean of the T_2 spectrum (ms)
T_{2i}	A variable relaxation time (ms)
t_m	Mean transmission travel time (s)
UCS	Uniaxial compressive strength (MPa)
V	Pore volume (μm^3)
V_{cal}	Volume of the calibration specimen (cm^3)
V_{ts}	Volume of the tested specimen (cm^3)
v_i	Coefficient of variation of t_{2i}
v_p	P-wave velocity (m/s)
W_i	Weight of pore size i
w_i	Weight of pore radius i before correction
w_{mac}	Weight of NMR amplitude of macro-pores
w_{mes}	Weight of NMR amplitude of meso-pores
w_{mic}	Weight of NMR amplitude of micro-pores
Δm	Mass loss (%)
ρ_d	Dry density (g/cm^3)
ρ_w	Water density (g/cm^3)
ρ_2	Transverse surface relaxivity (μm/ms)
ϕ_{cal}	Porosity of the calibration specimen (%)
ϕ	Porosity (%)
w	Water content (%)

References

Abdolghanizadeh, K., Hosseini, M., Saghafiyazdi, M., 2020. Effect of freezing temperature and number of freeze–thaw cycles on mode I and mode II fracture toughness of sandstone. Theor. Appl. Fract. Mech. 105, 102428.

Al-Omari, A., Beck, K., Brunetaud, X., Török, Á., Al-Mukhtar, M., 2015. Critical degree of saturation: a control factor of freeze–thaw damage of porous limestones at Castle of Chambord, France. Eng. Geol. 185, 71–80.

Auslander, M., Nevo, E., Inbar, M., 2003. The effects of slope orientation on plant growth, developmental instability and susceptibility to herbivores. J. Arid Environ. 55, 405–416.

Chen, T., Yeung, M., Mori, N., 2004. Effect of water saturation on deterioration of welded tuff due to freeze-thaw action. Cold Reg. Sci. Technol. 38, 127–136.

De Kock, T., Boone, M.A., De Schryver, T., Van Stappen, J., Derluyn, H., Masschaele, B., De Schutter, G., Cnudde, V., 2015. A pore-scale study of fracture dynamics in rock using X-ray micro-CT under ambient freeze–thaw cycling. Environ. Sci. Technol. 49, 2867–2874.

Deprez, M., De Kock, T., De Schutter, G., Cnudde, V., 2020. A review on freeze-thaw action and weathering of rocks. Earth Sci. Rev. 203, 103143.

Eslami, J., Walbert, C., Beaucour, A.L., Bourges, A., Noumowe, A., 2018. Influence of physical and mechanical properties on the durability of limestone subjected to freeze-thaw cycles. Construct. Build. Mater. 162, 420–429.

Fang, X., Xu, J., Wang, P., 2018. Compressive failure characteristics of yellow sandstone subjected to the coupling effects of chemical corrosion and repeated freezing and thawing. Eng. Geol. 233, 160–171.
Freire-Lista, D., Fort, R., Varas-Muriel, M., 2015. Freeze–thaw fracturing in building granites. Cold Reg. Sci. Technol. 113, 40–51.
Gao, F., Li, C., Xiong, X., Zhang, Y., Zhou, K., 2023. Dynamic behaviors of water-saturated and frozen sandstone subjected to freeze-thaw cycles. J. Rock Mech. Geotech. Eng. 15, 1476–1490.
GB/T 50266-2013, 2013. Standard for Tests Method of Engineering Rock Masses. China Planning Press, Beijing, China.
Guler, S., Türkmenoğlu, Z.F., Varol, O.O., 2021. Thermal shock and freeze-thaw resistance of different types of carbonate rocks. Int. J. Rock Mech. Min. Sci. 137, 104545.
Hale, P.A., Shakoor, A., 2003. A laboratory investigation of the effects of cyclic heating and cooling, wetting and drying, and freezing and thawing on the compressive strength of selected sandstones. Environ. Eng. Geosci. 9, 117–130.
Hall, K., 1999. The role of thermal stress fatigue in the breakdown of rock in cold regions. Geomorphology 31, 47–63.
Hou, C., Jin, X., He, J., Li, H., 2022. Experimental studies on the pore structure and mechanical properties of anhydrite rock under freeze-thaw cycles. J. Rock Mech. Geotech. Eng. 14, 781–797.
Huang, S., Lu, Z., Ye, Z., Xin, Z., 2020. An elastoplastic model of frost deformation for the porous rock under freeze-thaw. Eng. Geol. 278, 105820.
Huang, S., Yu, S., Ye, Y., Ye, Z., Cheng, A., 2022. Pore structure change and physico-mechanical proper- ties deterioration of sandstone suffering freeze-thaw actions. Construct. Build. Mater. 330, 127200.
Jia, H., Ding, S., Zi, F., Dong, Y., Shen, Y., 2020. Evolution in sandstone pore structures with freeze-thaw cycling and interpretation of damage mechanisms in saturated porous rocks. Catena 195, 104915.
Kenyon, W., Day, P., Straley, C., Willemsen, J., 1988. A three-part study of NMR longitudinal relaxation properties of water-saturated sandstones. SPE Form. Eval. 3, 622–636.
Khanlari, G., Abdilor, Y., 2015. Influence of wet–dry, freeze–thaw, and heat–cool cycles on the physical and mechanical properties of Upper Red sandstones in central Iran. Bull. Eng. Geol. Environ. 74, 1287–1300.
Li, A., Niu, F., Xia, C., Bao, C., Zheng, H., 2019. Water migration and deformation during freeze-thaw of crushed rock layer in Chinese high-speed railway subgrade: large scale experiments. Cold Reg. Sci. Technol. 166, 102841.
Li, J., Kaunda, R.B., Zhou, K., 2018a. Experimental investigations on the effects of ambient freeze-thaw cycling on dynamic properties and rock pore structure deterioration of sandstone. Cold Reg. Sci. Technol. 154, 133–141.
Li, J., Zhou, K., Liu, W., Zhang, Y., 2018b. Analysis of the effect of freeze–thaw cycles on the degradation of mechanical parameters and slope stability. Bull. Eng. Geol. Environ. 77, 573–580.
Lin, H., Lei, D., Zhang, C., Wang, Y., Zhao, Y., 2020. Deterioration of non-persistent rock joints: a focus on impact of freeze–thaw cycles. Int. J. Rock Mech. Min. Sci. 135, 104515.
Liu, T., Zhang, C., Cao, P., Zhou, K., 2020. Freeze-thaw damage evolution of fractured rock mass using nuclear magnetic resonance technology. Cold Reg. Sci. Technol. 170, 102951.
Luo, D., Jin, H., Bense, V.F., 2019. Ground surface temperature and the detection of permafrost in the rugged topography on ne Qinghai-Tibet Plateau. Geoderma 333, 57–68.
Luo, L., Pei, X., Pei, Z., Yang, B., Jin, Y., 2018. Distribution characteristics and susceptibility of talus slopes in the northern piedmont of Tianshan mountain. J. Catastrophology 33, 200–205.
Matsuoka, N., Sakai, H., 1999. Rockfall activity from an alpine cliff during thawing periods. Geomorphology 28, 309–328.
Meng, F., Zhai, Y., Li, Y., Zhao, R., Li, Y., Gao, H., 2021. Research on the effect of pore characteristics on the compressive properties of sandstone after freezing and thawing. Eng. Geol. 286, 106088.
Momeni, A., Abdilor, Y., Khanlari, G., Heidari, M., Sepahi, A., 2016. The effect of freeze–thaw cycles on physical and mechanical properties of granitoid hard rocks. Bull. Eng. Geol. Environ. 75, 1649–1656.
Mordovskoi, S., Petrov, E., 1994. Mechanical properties of frozen rock in a two-phase model. J. Min. Sci. 30, 48–53.
Mousavi, S.Z.S., Rezaei, M., 2022. Correlation assessment between degradation ratios of UCS and non-destructive properties of rock under freezing-thawing cycles. Geoderma 428, 116209.
Mousavi, S.Z.S., Tavakoli, H., Moarefvand, P., Rezaei, M., 2019. Assessing the effect of freezing-thawing cycles on the results of the triaxial compressive strength test for calc-schist rock. Int. J. Rock Mech. Min. Sci. 123, 104090.
Mousavi, S.Z.S., Tavakoli, H., Moarefvand, P., Rezaei, M., 2020a. Evaluating the variations of density and durability index of schist rock under the effect of freezing-thawing cycles. J. Min. Geol. 14, 1–12.
Mousavi, S.Z.S., Tavakoli, H., Moarefvand, P., Rezaei, M., 2020b. Micro-structural, petro-graphical and mechanical studies of schist rocks under the freezing-thawing cycles. Cold Reg. Sci. Technol. 174, 103039.
Özbek, A., 2014. Investigation of the effects of wetting–drying and freezing–thawing cycles on some physical and mechanical properties of selected ignimbrites. Bull. Eng. Geol. Environ. 73, 595–609.
Pan, Z., Zhou, K., Gao, R., Jiang, Z., Yang, C., Gao, F., 2020. Research on the pore evolution of sandstone in cold regions under freeze-thaw weathering cycles based on NMR. Geofluids 2020, 8849444.
Park, J., Hyun, C.U., Park, H.D., 2015. Changes in microstructure and physical properties of rocks caused by artificial freeze–thaw action. Bull. Eng. Geol. Environ. 74, 555–565.
Qin, L., Zhai, C., Liu, S., Xu, J., 2018. Mechanical behavior and fracture spatial propagation of coal injected with liquid nitrogen under triaxial stress applied for coalbed methane recovery. Eng. Geol. 233, 1–10.
Qin, L., Zhai, C., Liu, S., Xu, J., Yu, G., Sun, Y., 2017. Changes in the petrophysical properties of coal subjected to liquid nitrogen freeze-thaw – a nuclear magnetic resonance investigation. Fuel 194, 102–114.
Rezaee, R., Saeedi, A., Clennell, B., 2012. Tight gas sands permeability estimation from mercury injection capillary pressure and nuclear magnetic resonance data. J. Pet. Sci. Eng. 88–89, 92–99.
Ruedrich, J., Kirchner, D., Siegesmund, S., 2011. Physical weathering of building stones induced by freeze–thaw action: a laboratory long-term study. Environ. Earth Sci. 63, 1573–1586.
Sardana, S., Sinha, R.K., Verma, A., Jaswal, M., Singh, T., 2022a. Influence of freeze–thaw on the stability of road cut slopes—a case study in the Indian Himalayan region. Can. Geotech. J. 60, 107–112.
Sardana, S., Sinha, R.K., Verma, A., Singh, T., 2022b. Investigations into the freeze–thaw-induced alteration in microstructure and deteriorative responses of physico-mechanical properties of Himalayan rock. Bull. Eng. Geol. Environ. 81, 269.
Sass, O., 2005. Rock moisture measurements: techniques, results, and implications for weathering. Earth Surf. Process. Landforms 30, 359–374.
Sun, Y., Zhai, C., Xu, J., Cong, Y., Qin, L., Zhao, C., 2020. Characterisation and evolution of the full size range of pores and fractures in rocks under freeze-thaw conditions using nuclear magnetic resonance and three-dimensional X-ray microscopy. Eng. Geol. 271, 105616.
Verma, A., Sardana, S., Jaiswal, A., 2023. Study of freeze-thaw induced damage characteristic for Himalayan schist. J. Geol. Soc. India 99, 390–396.
Walbert, C., Eslami, J., Beaucour, A.L., Bourges, A., Noumowe, A., 2015. Evolution of the mechanical behaviour of limestone subjected to freeze–thaw cycles. Environ. Earth Sci. 74, 6339–6351.
Wan, X., Yang, Z.J., 2020. Pore water freezing characteristic in saline soils based on pore size distribution. Cold Reg. Sci. Technol. 173, 103030.
Wang, F., Cao, P., Wang, Y., Hao, R., Meng, J., Shang, J., 2020. Combined effects of cyclic load and temperature fluctuation on the mechanical behavior of porous sandstones. Eng. Geol. 266, 105466.
Weng, L., Wu, Z., Liu, Q., Chu, Z., Zhang, S., 2021. Evolutions of the unfrozen water content of saturated sandstones during freezing process and the freeze-induced damage characteristics. Int. J. Rock Mech. Min. Sci. 142, 104757.
Xie, R., Xiao, L., Wang, Z., Dunn, K.J., 2008. The influence factors of NMR logging porosity in complex fluid reservoir. Sci. China Earth Sci. 51, 212–217.
Yang, L., Jia, H., Han, L., Zhang, H., Tang, L., 2021. Hysteresis in the ultrasonic parameters of saturated sandstone during freezing and thawing and correlations with unfrozen water content. J. Rock Mech. Geotech. Eng. 13, 1078–1092.
Zhan, J., Chen, J., Zhang, W., Han, X., Sun, X., Bao, Y., 2018. Mass movements along a rapidly uplifting river valley: an example from the upper Jinsha River, southeast margin of the Tibetan Plateau. Environ. Earth Sci. 77, 1–18.
Zhang, S., Lai, Y., Zhang, X., Pu, Y., Yu, W., 2004. Study on the damage propagation of surrounding rock from a cold-region tunnel under freeze–thaw cycle condition. Tunn. Undergr. Space Technol. 19, 295–302.

Xiaoyan Zhao is a professor of Geological Resources and Geological Engineering at Southwest Jiaotong University. He obtained his BSc degree and PhD in Geological Engineering from Southwest Jiaotong University, China, in 2000 and 2005, respectively. He is an executive member of the Transportation Branch of China Association for Disaster Prevention. His research interests include (1) Rock weathering and geomorphic processes; (2) Prevention and control of collapse and rockfall; and (3) Engineering geological survey and route selection for railway.

Please cite this article as: Xiao D et al., Effects of freeze-thaw cycles on sandstone in sunny and shady slopes, Journal of Rock Mechanics and Geotechnical Engineering, https://doi.org/10.1016/j.jrmge.2023.12.023